Journal of Materials Science: Materials in Electronics (2018) 29:9077–9082
https://doi.org/10.1007/s10854-018-8934-2

High performance back-illuminated MIS structure AlGaN solar-blind ultraviolet photodiodes

W. Y. Han[1,2] · Z. W. Zhang[1] · Z. M. Li[1] · Y. R. Chen[1] · H. Song[1] · G. Q. Miao[1] · F. Fan[1,2] · H. F. Chen[1,2] · Z. Liu[1,2] · H. Jiang[1]

Received: 4 December 2017 / Accepted: 15 March 2018 / Published online: 16 March 2018

Abstract
A back-illuminated metal–insulator–semiconductor (MIS) structure AlGaN-based solar-blind ultraviolet photodiode is demonstrated for the purpose of overcoming the technical bottleneck caused by high Al content p-AlGaN in p–i–n structure. The device presents a peak responsivity of 0.115 A/W at 270 nm, corresponding to an external quantum efficiency (EQE) of 53% and an ultraviolet/visible rejection ratio of more than three orders of magnitude under zero-bias. Moreover, a response speed around 24 μs and a peak responsivity of 0.154 A/W, corresponding to an EQE of 70.6% will be achieved at a reverse bias of 3 V. The excellent performances of the back-illuminated MIS photodetector can be attributed to the adoption of a thin n-AlGaN layer of Al content gradient which plays a role of completely relaxing the strain of light absorption layer and the introduction of a homogeneous n-AlGaN interlayer into light absorption region which redistributes its electric field in favor of the separation and transport of the photo-generated carriers.

1 Introduction

The ozone layer in the atmosphere can absorb nearly 100 percent of the wavelengths of solar radiation shorter than 280 nm, which creates a natural low terrestrial background called solar-blind region [1]. Within this region, the development of related high-efficiency solar-blind ultraviolet photodetectors (UV-PDs) has drawn more and more attention for their potential applications in early missile threat warning, missile guidance, covert space-to-space communication, secure non line-of-sight communication, flame monitoring, ultrahigh voltage leakage corona monitoring, bioagent detection, UV environmental monitoring, UV astronomy, and so on [2–4]. Among a series of wide bandgap semiconductors, the ternary AlGaN alloy is considered to be one of the most ideal materials for developing solar-blind UV-PDs, because it has a tunable bandgap which ranges from 3.4 to 6.2 eV (the corresponding absorption wavelength covers from 365 to 200 nm), sharp cut-off wavelength, full solid-state and high signal to background ratio, in addition to its excellent chemical and thermal stability [5, 6]. The AlGaN alloy with Al content higher than 40% will work in solar-blind region. In traditional studies, researchers are focusing on the back-illuminated p–i–n structure AlGaN-based UV-PD, because of its intrinsic advantages: low dark current, high response speed, and apt to integrate with the Si-based readout integrated circuit (ROIC) using flip-chip technique to make focal plane arrays [7, 8]. However, it also has lots of shortcomings: (i) high performance p-type doping AlGaN with high Al content is difficult to obtain, as a result of the high activation energy for the passive acceptors of the magnesium atoms. (ii) This material suffers from lattice mismatch and thermal expansion mismatch, because of the difference for lattice constant and thermal expansion coefficient between the sapphire substrate and the epitaxial layer, which will lead to cracks in epilayer. (iii) It is difficult to form good ohmic contact on p-AlGaN that affects the transport of photon-generated carriers [9]. Although p-GaN can be adopted to overcome the influence of the poor performance p-AlGaN and solve the transport problem of photo-generated carriers, the introduction of p-GaN layer will enable the device to have a spectral response at the near-ultraviolet band, which does not fully meet the requirement of the solar-blind UV-PD [10]. Fortunately, the back-illuminated

✉ Y. R. Chen
chenyr@ciomp.ac.cn

✉ H. Jiang
jiangh@ciomp.ac.cn

[1] State Key Laboratory of Luminescence and Applications, Changchun Institute of Optics, Fine Mechanics and Physics, Chinese Academy of Sciences, Changchun 130033, China

[2] University of Chinese Academy of Sciences, Beijing 100039, China

metal-insulator-semiconductor (MIS) structure AlGaN-based photodiode not only has the same advantages as the p–i–n structure photodiode, but also avoids its disadvantages, because it replaces high Al content p-type AlGaN material with a high work function metal electrode, which is thus promising to solve the technical bottleneck caused by p-AlGaN.

In recent, for the purpose of overcoming the limitation arose from the pivotal problem of achieving a high hole concentration and subsequently a low-resistivity p-type AlGaN film with high Al content, Liang et al. successfully circumvented the p-type AlGaN layer of a deep ultraviolet light-emitting diode (LED) by implementing with a MIS structure. The LED operated as a Schottky diode and presented a lower threshold voltage [11]. This further confirms that the back-illuminated MIS structure AlGaN-based UV-PDs, as one kind of Schottky photodiodes, will be an attractive choice for solar-blind photodetectors. However, so far, the studies on back-illuminated solar-blind AlGaN-based Schottky photodiodes mainly concentrate on the planar metal–semiconductor–metal (MSM) structure. Yang et al. have fabricated a back-illuminated solar-blind AlGaN-based photodetector based on planar MSM structure and obtained an EQE as high as 48% and a responsivity of 100 mA/W under − 100 V [12]. Huang et al. also have developed a back-illuminated solar-blind Schottky photodiode based on planar MSM structure using intrinsic $Al_{0.4}Ga_{0.6}N$ material as a light absorption layer, which presented a bandpass spectral response ranging from 244 to 275 nm with a peak responsivity of 98 mA/W at 262 nm and zero bias, corresponding to an EQE of 46% [13]. Sang et al. have reported a back-illuminated AlGaN solar-blind Schottky photodiode which presented a peak responsivity only 26 mA/W and an ultraviolet/visible rejection ratio of 1000 at 289 nm and zero bias [14]. The development lag of back-illuminated solar-blind AlGaN-based Schottky photodiodes can be ascribed to the reason that their spectral response and EQE are always poorer than that of back-illuminated p–i–n junctions due to the smaller built-in electric field of Schottky diodes and the narrower depletion region. Therefore, the effective method to solve the problems mentioned above is to introduce an insulating layer into the metal–semiconductor interface of Schottky diode and form an MIS structure. However, there are few reports on the back-illuminated MIS structure AlGaN-based solar-blind UV-PDs.

In this letter, an improved back-illuminated MIS structure AlGaN-based UV-PD is demonstrated for the purpose of overcoming the technical bottleneck caused by high Al content p-AlGaN of p–i–n structure. The insulating layer is in-situ grown by metal–organic chemical vapor deposition (MOCVD). Distinguished from the conventional MIS structure, a thin n-AlGaN with Al content gradually decreasing from 0.54 to 0.45 is used as an interlayer of the heterojunction. In addition, a homogeneous n-AlGaN interlayer is introduced into the i-AlGaN insulating layer.

2 Experimental

2.1 Preparation of the epitaxial material

A schematic cross-section of the device is shown in Fig. 1a. The epitaxial material of back-illuminated MIS structure solar-blind UV-PD was grown by low-pressure MOCVD on a 2-inch c-plane sapphire substrate. Trimethylaluminium (TMAl), trimethylgallium (TMGa) and ammonia (NH_3) were used as the precursors for Al, Ga and N sources respectively, and hydrogen (H_2) was the carrier gas. Silane (SiH_4) was used as the n-type dopant. Deposition was initiated with the AlN buffer layer grown by optimized growth conditions [15], followed by a ten periods of $Al_{0.58}Ga_{0.42}N$/AlN superlattices (SLs) layer releasing the stress formed by lattice mismatch and thermal expansion mismatch between

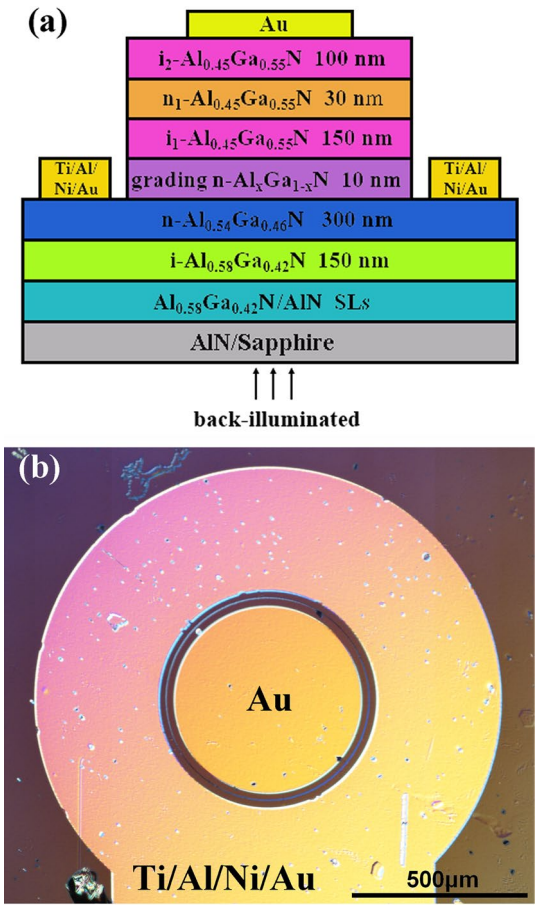

Fig. 1 **a** Schematic configuration of the back-illuminated MIS structure AlGaN-based solar-blind UV-PD. **b** The metallographic micrograph of a physical cell

AlN and following AlGaN and suppressing the dislocations extension from the AlN template to the AlGaN [16]. Then, a 150 nm-thick undoped $Al_{0.58}Ga_{0.42}N$ layer was grown on top of the SLs layer. Both of the SLs and the undoped $Al_{0.58}Ga_{0.42}N$ layers were grown at 1180 °C with a reactor pressure of 50 mbar and a V/III ratio of about 50. In the group-III, the molar ratio between TMAl and TMGa was 5. Next, it was followed by the insulator-semiconductor structure consisting of a 300 nm-thick silicon doped n-$Al_{0.54}Ga_{0.46}N$ ($n \sim 1 \times 10^{18}$ cm^{-3}) layer, a 10 nm-thick grading n-$Al_xGa_{1-x}N$ layer with Al content decreasing from 54 to 45%, a 150 nm-thick undoped i_1-$Al_{0.45}Ga_{0.55}N$ layer, a 30 nm-thick n_1-$Al_{0.45}Ga_{0.55}N$ layer ($n \sim 1 \times 10^{18}$ cm^{-3}) and a 100 nm-thick undoped i_2-$Al_{0.45}Ga_{0.55}N$ layer. All of these layers were grown at 1160 °C with a reactor pressure of 50 mbar. Among them, the V/III ratio of the n-$Al_{0.54}Ga_{0.46}N$ layer was about 50 while that of the n-$Al_xGa_{1-x}N$ layer with Al content decreasing from 54 to 45% was gradually changing from 50 to 40 by increasing the TMGa source and adjusting the molar ratio between TMAl and TMGa from 5 to 4. In addition, the V/III ratios of the other layers, such as the i_1-$Al_{0.45}Ga_{0.55}N$, n_1-$Al_{0.45}Ga_{0.55}N$ and i_2-$Al_{0.45}Ga_{0.55}N$ layers were kept at 40.

2.2 Device fabrication

The metallographic micrograph of a physical back-illuminated MIS structure AlGaN-based UV-PD cell is shown in Fig. 1b. In the device fabrication process, firstly, the inductively coupled plasma (ICP) dry etching was used to etch the material to the n-$Al_{0.54}Ga_{0.46}N$ layer and formed a 500 μm-diameter mesa. In the etching process of the ICP, the Cl_2 (8 sccm)/BCl_3 (24 sccm) with Ar (6 sccm) and He (4 sccm) as additive gases were adopted as the plasma mixtures while the ICP power and the reactive pressure were 700 W and 0.55 Pa, respectively. Secondly, the sample was treated by a photo-electrochemical method to remedy the damage made by ICP etching, reducing the dark current [17]. Then, a Ti/Al/Ni/Au (30/100/150/200 nm) ring electrode was deposited onto the n-$Al_{0.54}Ga_{0.46}N$ using electron-beam evaporation and standard lift-off technique based on photolithography and annealed at 500 °C for 60 s in N_2 ambient by rapid thermal annealing system to realize ohmic contact. At last, a 200 nm-thick circle Au electrode was similarly deposited onto the i_2-$Al_{0.45}Ga_{0.55}N$ layer by electron-beam evaporation and standard lift-off technique.

2.3 Characterizations

The asymmetrical reciprocal space mapping (RSM) around the $(10\bar{1}5)$ reflection was characterized by high-resolution X-ray diffractometer (HRXRD, Bruker D8). The current–voltage (I–V) property of the MIS device at room temperature was measured by using a semiconductor parameter analyzer (Agilent B1500A). A calibrated UV spectral response test system with a 200 W UV-enhanced Xe lamp and a monochromator was used to obtain the spectral response properties of the MIS photodetector. The transient spectral response of the photodetector was stimulated by a 10 mW Nd:YAG laser (266 nm) and recorded by an oscilloscope (Tektronix DPO 5104 digital oscilloscope). The electric field profiles were calculated using a commercial simulator (APSYS).

3 Results and discussion

To evaluate the crystalline quality of the epitaxial material, the asymmetrical RSM is measured around $(10\bar{1}5)$ reflection, as shown in Fig. 2. Each reciprocal lattice point (RLP) shown in the RSM represents each epilayer. The RLPs mainly correspond to the AlN buffer layer, the $Al_{0.58}Ga_{0.42}N$/AlN superlattices (SLs) layer, the i-$Al_{0.58}Ga_{0.42}N$ layer, the n-$Al_{0.54}Ga_{0.46}N$ layer and the $Al_{0.45}Ga_{0.55}N$ layer, which are consistent with the material structure of Fig. 1a. The RLP corresponding to the thin n-AlGaN gradient layer is shown in Fig. 2 marked by the white circle. It should be noted that the homogeneous n-$Al_{0.45}Ga_{0.55}N$ interlayer has the same Al content as the i-$Al_{0.45}Ga_{0.55}N$ layer, which cannot be distinguished from the RLP of $Al_{0.45}Ga_{0.55}N$. In Fig. 2, q_x and q_z are stood for the directions parallel and vertical to the interface between epilayer and substrate, which are mainly used to calculate the in-of-plane and out-of-plane lattice constants through [18].

$$a = (4(h^2 + hk + k^2)/3q_x^2)^{1/2}, \tag{1}$$

$$c = l/q_z, \tag{2}$$

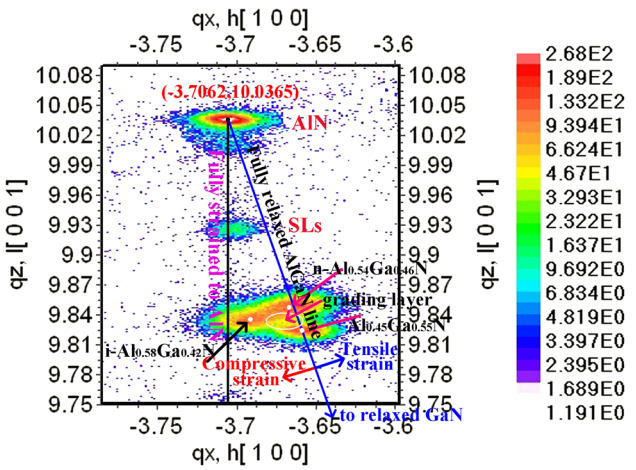

Fig. 2 The asymmetrical reciprocal space mapping around $(10\bar{1}5)$ reflection for epitaxial material by HRXRD

where *h, k*, and *l* are the Miller indices. The lattice constants for relaxed AlN are (a = 0.31127 nm, c = 0.49817 nm). Therefore, the RLP denoted as (q_x, q_z) for the relaxed AlN can be calculated as (− 3.7096, 10.0367) for $(10\bar{1}5)$ reflection. In this paper, the RLP of the optimized AlN buffer layer is (− 3.7062, 10.0365) which means that the AlN buffer layer is almost relaxed. As seen in Fig. 2, the connection line (blue one) extended from the RLP of the fully relaxed AlN to the fully relaxed GaN will represent fully relaxed $Al_xGa_{1-x}N$ while the connection line (black one) represents $Al_xGa_{1-x}N$ fully strained to AlN. It should be noted that the RLP of the relaxed GaN is beyond the coordinates in Fig. 2. It has been concluded that the region (indicated by the red arrow) to the left side of the fully relaxed $Al_xGa_{1-x}N$ line represents $Al_xGa_{1-x}N$ under compressive strain while the region (indicated by the blue arrow) to the right side represents $Al_xGa_{1-x}N$ under tensile strain [18]. Therefore, as can be seen, the RLPs of the i-$Al_{0.58}Ga_{0.42}N$ layer and the n-$Al_{0.54}Ga_{0.46}N$ layer (white points) locate at the left side of the fully relaxed $Al_xGa_{1-x}N$ line which means that both of them present compressive strain. Obviously, the RLP of the n-$Al_{0.54}Ga_{0.46}N$ layer is closer to the fully relaxed $Al_xGa_{1-x}N$ line than that of the i-$Al_{0.58}Ga_{0.42}N$ layer, indicating the smaller compressive strain in n-$Al_{0.54}Ga_{0.46}N$ layer, which quite agrees with the Si doping effect on strain reduction in compressive strained AlGaN thin films demonstrated by Cantu et al. [19]. Learned from the asymmetrical RSM around $(10\bar{1}5)$ reflection, the introduction of a thin n-AlGaN gradient layer as the transition layer between n-$Al_{0.54}Ga_{0.46}N$ and i_1-$Al_{0.45}Ga_{0.55}N$ will further regulate the strain of the following epitaxial layers, and thus obtain fully relaxed i_1-$Al_{0.45}Ga_{0.55}N$/n_1-$Al_{0.45}Ga_{0.55}N$/i_2-$Al_{0.45}Ga_{0.55}N$ homogeneous multilayer, whose RLP locates at the fully relaxed $Al_xGa_{1-x}N$ line. In short, we first grow epitaxial materials that meet the structural design on the optimized AlN template, and prepare the fully relaxed homogeneous multilayer as the light absorption layer by introducing the n-AlGaN gradient layer. The fully relaxed light absorption layer contains an n-$Al_{0.45}Ga_{0.55}N$ interlayer.

The back-illuminated MIS structure solar-blind UV-PD is fabricated based on the structural epitaxial material, as shown in Fig. 1b. The detailed fabrication process of the device has been described in the Sect. 2. The dark current–voltage (*I–V*) characteristic is shown in Fig. 3a using a semi-log coordinate. It can be seen that the *I–V* characteristic has the same good rectifying behavior as that of the p–i–n structure. The dark current density is about 2.4×10^{-7} A/mm^2 under 3 V reverse bias. The spectral responsivity and the corresponding external quantum efficiency (EQE) under different bias are measured by a calibrated UV-enhanced spectral response test system, as shown in Fig. 3b and inset. It presents a bandpass response characteristic with a range from 255 to 280 nm, which is completely in conformity with

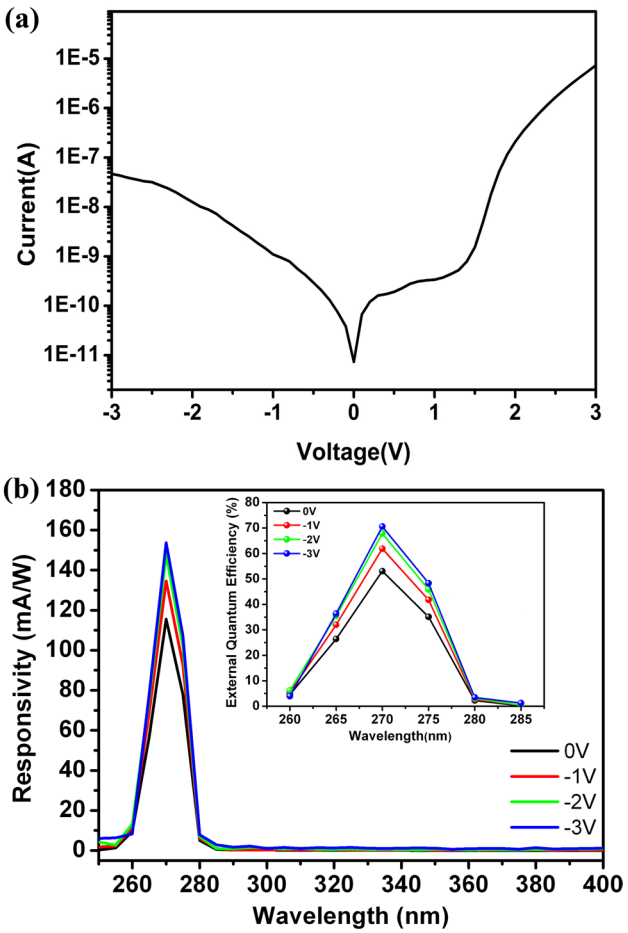

Fig. 3 **a** The dark current characteristic curve of the MIS structure solar-blind UV-PD in a semi-log coordinate. **b** Spectral responsivity curves under different bias. The inset shows the corresponding EQE values versus wavelengths

solar-blind UV detection. The peak responsivity at zero bias locates at 270 nm with a value of 0.115 A/W, corresponding to a high EQE of 53%, and the ultraviolet/visible rejection ratio is more than three orders of magnitude. Moreover, the responsivity increases to 0.154 A/W, corresponding to an EQE of 70.6% under − 3 V, which is relatively higher than those of the reported AlGaN solar-blind Schottky photodiodes.

Figure 4 shows the transient spectral response of the device at reverse bias of 3 V which is stimulated by a pulsed Nd:YAG laser with a 266 nm wavelength (the laser pulse width is 10 ns) and measured by a Tektronix DPO 5104 digital oscilloscope. The 10–90% rise time (defined as the time for the photocurrent increasing from 10 to 90% of the peak value) of the device is around 1.4 ns while the 90–10% decay time (defined as the time for the photocurrent dropping from 90 to 10% of the peak value) is around 55 μs. We fit the decay section of Fig. 4 with an exponential decay curve, and a good fitting is accomplished by using a first-order

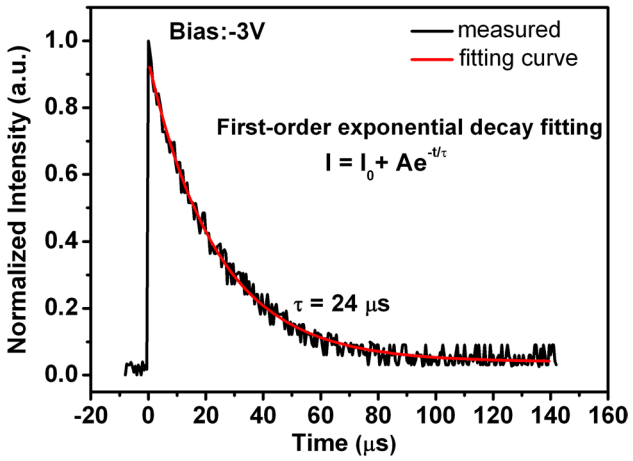

Fig. 4 Decay edge of the transient spectral response at reverse bias of 3 V

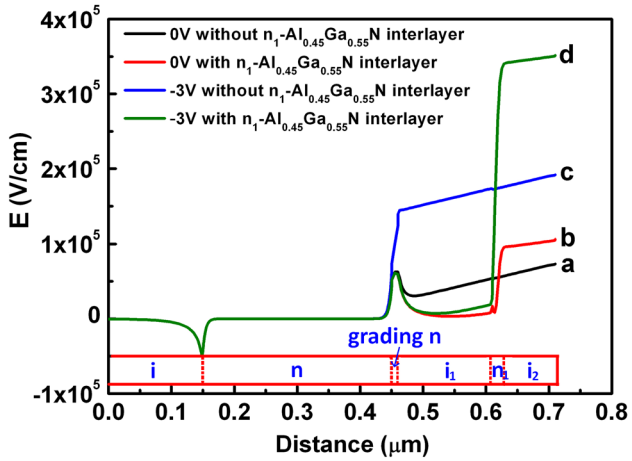

Fig. 5 Distribution of the electric field in the MIS structure AlGaN-based solar-blind UV-PD with and without an n_1-$Al_{0.45}Ga_{0.55}N$ interlayer

exponential decay function. The fitting decay time is around 24 μs. Due to the introduction of the intrinsic absorption layer into the Schottky photodiode to form the MIS structure, its response speed will greatly limit by the increasing RC constant. As far as we known, the response speed of our device is by far the quickest one among the reported back-illuminated MIS structure AlGaN-based solar-blind UV-PD.

The high performance of the back-illuminated MIS structure AlGaN-based solar-blind UV-PD can be attributed to the strong electric field (E) in the light absorption layer due to the introduction of the n_1-$Al_{0.45}Ga_{0.55}N$ interlayer, in addition to the quality improvement of the epitaxial material by the n-AlGaN gradient layer. A strong E within the light absorption layer can improve the separation and transport of the photo-generated carriers. The result is to reduce carrier recombination, increase the extraction of the photoelectric current and improve the response speed as well. In order to confirm this viewpoint, the electric field profiles of the MIS structure AlGaN-based solar-blind UV-PD with and without an n_1-$Al_{0.45}Ga_{0.55}N$ interlayer are analyzed by a commercial simulator, APSYS.

In Fig. 5a and c represent the electric field profiles of the MIS device without an n_1-$Al_{0.45}Ga_{0.55}N$ interlayer under 0 V and − 3 V, respectively. Similarly, b and d represent the electric field profiles of the MIS device with an n_1-$Al_{0.45}Ga_{0.55}N$ interlayer under 0 V and − 3 V, respectively. It should be noted that the bandpass spectral response characteristic of the back-illuminated photodetector has cutoff wavelengths in both short wavelength and long wavelength sides, which are determined by the window layer and the light absorption layer, respectively [1, 10]. In this paper, the window layer is mainly determined by the bottom i-$Al_{0.58}Ga_{0.42}N$, n-$Al_{0.54}Ga_{0.46}N$ and Al content gradient n-AlGaN layers while the light absorption layer mainly consists of i_1-$Al_{0.45}Ga_{0.55}N$, n_1-$Al_{0.45}Ga_{0.55}N$ and i_2-$Al_{0.45}Ga_{0.55}N$ layers.

Obviously, the structure with the n_1-$Al_{0.45}Ga_{0.55}N$ layer presents higher electric field in the light absorption section than that without the n_1-$Al_{0.45}Ga_{0.55}N$ layer no matter the device is under reverse bias or not. In fact, the back-illuminated MIS device with an n-AlGaN interlayer in the light absorption region is to some extent similar to the back-illuminated separate absorption and multiplication (SAM) structure p–i–n photodiode which has been proved to be an effective way to improve the performance of the photodetectors [13, 20]. In other words, the introduction of the n_1-$Al_{0.45}Ga_{0.55}N$ interlayer indeed realizes the electric field of the light absorption region to redistribute and make for the separation and transport of the photo-generated carriers. Therefore, the device presents excellent responsivity and EQE.

4 Conclusions

In summary, a back-illuminated MIS structure AlGaN-based solar-blind UV-PD has been intensively demonstrated. The peak responsivity of 0.115 A/W was obtained at 270 nm under zero-bias, corresponding to an EQE of 53% while that increases to 0.154 A/W, corresponding to an EQE of 70.6% under − 3 V. Moreover, the rise time and the decay time of the device are only 1.4 ns and 24 μs, respectively. The relatively excellent performances of the MIS photodetector can be ascribed to the optimized structural design. The thin Al content gradient n-AlGaN located at the interface of the heterojunction plays the role of further regulating the strain of the following epitaxial layers, and thus the fully relaxed light absorption layer is obtained. The presence of the homogenous n-AlGaN interlayer redistributes the electric field of the light absorption region in favor of the separation and transport of the photo-generated carriers. The development

of high performance back-illuminated MIS structure solar-blind UV-PD will benefit to overcome the technical bottleneck caused by high Al content p-AlGaN in the p–i–n structure AlGaN solar-blind ultraviolet photodetector.

Acknowledgements This work was partially supported by the National Natural Science Foundation of China (Grant Nos. 61504144 and 51472230), and the Jilin Provincial Science & Technology Department (Grant No. 20170520156JH).

References

1. R. McClintock, M. Razeghi, Solar–blind photodetectors and focal plane arrays based on AlGaN. Proc. SPIE **9555**, 955502 (2015)
2. M. Razeghi, Short–wavelength solar–blind detectors–status, prospects, and markets. Proc. IEEE **90**, 1006–1014 (2002)
3. L.W. Sang, M.Y. Liao, M. Sumiya, A comprehensive review of semiconductor ultraviolet photodetectors: from thin film to one–dimensional nanostructures. Sensors **13**, 10482–10518 (2013)
4. E. Cicek, R. McClintock, Z. Vashaei, Y. Zhang, S. Gautier, C.Y. Cho, M. Razeghi, Crack–free AlGaN for solar–blind focal plane arrays through reduced area epitaxy. Appl. Phys. Lett. **102**, 051102 (2013)
5. M.A. Khan, M. Shatalov, H.P. Maruska, H.M. Wang, E. Kuokstis, III–nitride UV devices. Jpn. J. Appl. Phys. **44**, 7191–7206 (2005)
6. J.Q. Zhang, Y.T. YangV, H.J. Jia, AlGaN metal–semiconductor–metal ultraviolet photodetectors on sapphire substrate with a low–temperature AlN buffer layer. Chin. Opt. Lett. **11**, 102304–102306 (2013)
7. E. Monroy, F. Calle, E. Muñoz, F. Omnès, AlGaN metal–semiconductor–metal photodiodes. Appl. Phys. Lett. **74**, 3401–3403 (1999)
8. G.Y. Xu, A. Salvador, W. Kim, Z. Fan, C. Lu, H. Tang, H. Morkoç, G. Smith, M. Estes, B. Goldenberg, W. Yang, S. Krishnankutty, High speed, low noise ultraviolet photodetectors based on GaN p–i–n and AlGaN(p)–GaN(i)–GaN(n) structures. Appl. Phys. Lett. **71**, 2154–2156 (1997)
9. T. Li, A.L. Beck, C. Collins, R.D. Dupuis, J.C. Campbell, J.C. Carrano, M.J. Schurman, I.A. Ferguson, Improved ultraviolet quantum efficiency using a semitransparent recessed window AlGaN/GaN heterojunction p–i–n photodiode. Appl. Phys. Lett. **75**, 2421–2423 (1999)
10. D.G. Zhao, S. Zhang, D.S. Jiang, J.J. Zhu, Z.S. Liu, H. Wang, S.M. Zhang, B.S. Zhang, H. Yang, A study on the spectral response of back–illuminated p–i–n AlGaN heterojunction ultraviolet photodetector. J. Appl. Phys. **110**, 053701 (2011)
11. Y.-H. Liang, E. Towe, Low–threshold voltage ultraviolet light–emitting diodes based on (Al,Ga)N metal–insulator–semiconductor structures. Appl. Phys. Express **10**, 121005 (2017)
12. K. Baba, T. Yonezawa, M. Miyagi, Metal island films for write–once multiwavelength three–dimensional optical disks. Electron. Lett. **36**, 1865 (2000)
13. Z.Q. Huang, J.F. Li, W.L. Zhang, H. Jiang, AlGaN solar–blind avalanche photodiodes with enhanced multiplication gain using back–illuminated structure. Appl. Phys. Express **6**, 054101 (2013)
14. L.W. Sang, Z.X. Qin, L.B. Cen, B. Shen, G.Y. Zhang, S.P. Li, H.Y. Chen, D.Y. Liu, J.Y. Kang, C.J. Cheng, H.Y. Zhao, Z.X. Lu, J.X. Ding, L. Zhao, J.J. Si, W.G. Sun, AlGaN–based solar–blind Schottky photodetectors fabricated on AlN/sapphire template. Chin. Phys. Lett. **25**, 258–261 (2008)
15. Y.R. Chen, H. Song, D.B. Li, X.J. Sun, H. Jiang, Z.M. Li, G.Q. Miao, Z.W. Zhang, Y. Zhou, Influence of the growth temperature of AlN nucleation layer on AlN template grown by high-temperature MOCVD. Mater. Lett. **114**, 26–28 (2014)
16. E. Cicek, R. Mcclintock, C.Y. Cho, B. Rahnema, M. Razeghi, $Al_xGa_{1-x}N$–based solar–blind ultraviolet photodetector based on lateral epitaxial overgrowth of AlN on Si substrate. Appl. Phys. Lett. **103**, 181113 (2013)
17. D.B. Li, X.J. Sun, H. Song, Z.M. Li, Y.R. Chen, G.Q. Miao, H. Jiang, Influence of threading dislocations on GaN–based metal–semiconductor–metal ultraviolet photodetectors. Appl. Phys. Lett. **98**, 011108 (2011)
18. A. Kadir, C.C. Huang, K.E.K. Lee, E.A. Fitzgerald, S.J. Chua, Determination of alloy composition and strain in multiple AlGaN buffer layers in GaN/Si system. Appl. Phys. Lett. **105**, 232113 (2014)
19. P. Cantu, F. Wu, P. Waltereit, S. Keller, A.E. Romanov, U.K. Mishra, S.P. DenBaars, J.S. Speck, Si doping effect on strain reduction in compressively strained $Al_{0.49}Ga_{0.51}N$ thin films. Appl. Phys. Lett. **83**, 674 (2003)
20. H.F. Chen, Y.R. Chen, H. Song, Z.M. Li, H. Jiang, D.B. Li, G.Q. Miao, X.J. Sun, Z.W. Zhang, Dependence of dark current and photoresponse on polarization charges for AlGaN–based heterojunction p–i–n photodetectors. Phys. Status Solidi A **214**, 1600932 (2017)